J. Fluid Mech. (1980), *vol.* 97, *part* 3, *pp.* 455–479
Printed in Great Britain

The spectral characteristics of wind-generated capillary waves

By G. T. LLEONART† AND DEANE R. BLACKMAN
Department of Mechanical Engineering, Monash University, Australia

(Received 5 October 1978 and in revised form 20 April 1979)

An experimental study of wind-generated capillary waves has been carried out in a laboratory wind–wave tunnel. In this tunnel it was possible to generate a stationary homogeneous wave field and to vary the wind over a range of speeds. A technique which makes use of a Preston tube has been used to measure the shear stress at the air–water boundary. Measurements of surface elevation and wave slope spectra in the capillary range of frequencies were obtained. Equations describing the wave spectra equilibrium range under the action of wind shear, surface tension and viscosity are derived. For frequencies beyond 15 hertz the measured spectra are in satisfactory agreement with the derived equations. Comparisons with other existing data have also been made.

1. Introduction

The manner in which surface waves are generated and sustained by wind blowing over water is a topic of longstanding interest to oceanographers. There have been many theoretical and experimental studies concerned with wind-generated gravity waves, but attempts to obtain detailed observations of capillary waves generated by wind have been comparatively rare. High frequency waves, i.e. capillary and gravity–capillary waves, are thought to play a significant role in a number of physical processes associated with air–sea interactions; examples include: transfer of momentum from wind to waves, aerodynamic roughness of the water surface, water vapour diffusion at the ocean surface, nonlinear wave interactions and backscatter of electromagnetic radiation from the sea surface. In engineering processes involving two-phase flows, where capillary waves form at gas–liquid interfaces, they exert considerable influence on heat and mass transfer coefficients.

To date little success has attended efforts to expose the properties of capillary waves generated by wind. In an endeavour to gain a better understanding of the nature of these waves, we have undertaken a study aimed at exploring the characteristics of the wave disturbed surface as well as the wind flow over the waves. In this report we will deal, principally, with the spectral characteristics of capillary waves. The experimental apparatus and techniques used to make observations of wave elevation and wave slope are described, and equations pertaining to wave spectra in the saturation range are given and compared with observations.

Our experimental approach, which we outline briefly, was to seek a simplification of the natural, uncontrolled conditions of wind blowing over water in such a way that

† Present address: Footscray Institute of Technology, Ballarat Road, Footscray, Victoria, Australia.

0022–1120/80/4408–8540 $02.00

we could isolate capillary waves and study their properties in the laboratory. Certain experimental advantages result if a stationary homogeneous wave field can be produced. In order to achieve homogeneity we have chosen to generate the waves within a long rectangular channel of large aspect ratio. Provided the mean depth of water covering the floor was held constant during wave generation, we have found that a two-dimensional shear flow of air displays a constant pressure gradient, thus indicating that both the wind field and wave field are stationary and homogeneous.

The wind generates a band of wave frequency components, and although it is expected that the dominant waves will be influenced by the depth of water in the channel there should nevertheless exist a range of waves of shorter length and higher frequency that are unaffected by the depth limitation. To estimate the length of a capillary wave free from depth affects we may use the results of Crapper (1957) who, considering solely the influence of surface tension, found a theoretical solution describing finite-amplitude capillary waves. For waves on water these waves have lengths up to approximately 5 mm. Assuming deep-water waves are those standing on water whose depth exceeds one-half wavelength, we may anticipate for experiments conducted in water 5 mm deep that deep water waves about 1 cm long are possible.

To distinguish between wavenumbers influenced by surface tension or gravity, Phillips (1966) uses a wavenumber, k_γ, which gives equal weight to each force,

$$k_\gamma = (g/\gamma)^{\frac{1}{2}}; \tag{1}$$

here g is the gravitational acceleration and γ the ratio of surface tension to fluid density. It is instructive to compare the surface-tension forces to the gravitational forces for a given wavelength, λ, by writing their ratio, r, in the form,

$$r = \frac{\gamma}{g}\left(\frac{2\pi}{\lambda}\right)^2. \tag{2}$$

For water waves 1 cm long on deep water (2) shows that the surface-tension forces are three times the gravitational forces. Clearly there are no definite boundaries for spectral ranges, but in order to estimate a lower frequency limit of the capillary-wave spectrum in water 5 mm deep, we assume waves less than 1 cm long are capillary. Under this assumption the lower frequency limit is about 25 Hz. Therefore, effective measurements of capillary-wave spectra under the conditions described above require wave sensors capable of resolving wave frequencies well in excess of 25 Hz.

A number of laboratory experiments have demonstrated that for turbulent wind blowing over small gravity–capillary waves the velocity profile in the air is well described by a logarithmic distribution. The air flow in our channel, which was fully-developed shear flow, can therefore be satisfactorily characterized by the friction velocity $u_* = (\tau_w/\rho)^{\frac{1}{2}}$, where τ_w is the shear stress at the air–water boundary and ρ is the density of air. Another feature associated with using the channel flow to generate the wave field is that it allows the use of a sound method for measuring τ_w.

2. Equipment and experimental procedure

Wind–wave tunnel

A diagram of the wind–wave tunnel is shown in figure 1. The tunnel, 12 m long and of cross-section 32 × 560 mm, sits within a concrete flume 30 m long and 60 cm square in

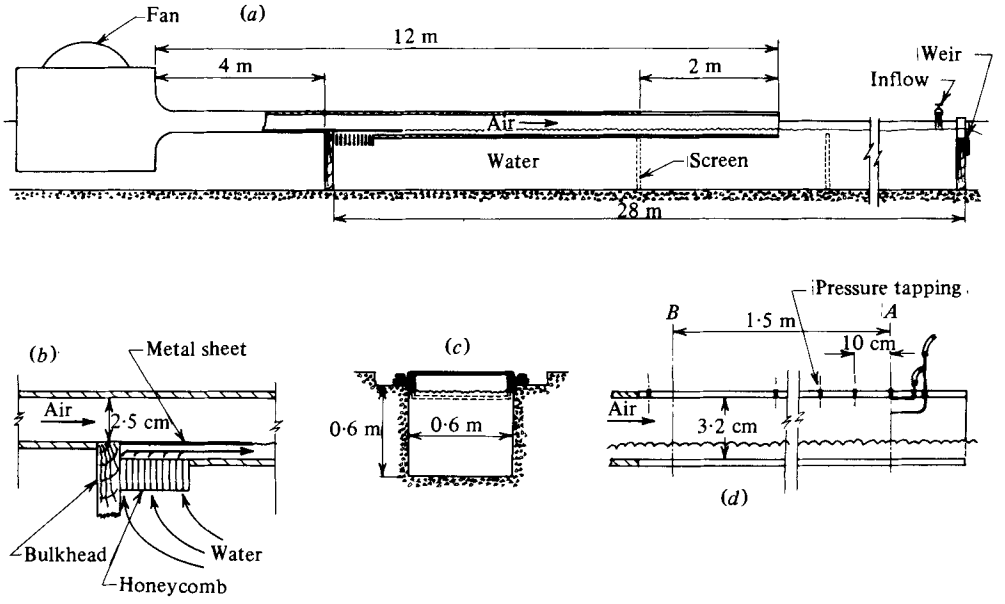

FIGURE 1. The wind–wave tunnel. (*a*) Arrangement of tunnel in flume. (*b*) Detail of water entry. (*c*) Cross-section. (*d*) Detail of working section.

section. It rests at one end on a bulkhead and is supported elsewhere by adjustable legs such that its longitudinal axis may be inclined slightly from the horizontal. A centrifugal fan was used to drive air into a plenum chamber, then through a contraction into the tunnel proper. The flow was controlled by a baffle situated at the fan inlet. A working section 2 m long was fabricated from braced perspex sheets and static pressure tappings, 0·4 mm diameter, spaced at 10 cm intervals, were inserted along the centre-line of the top wall of the working section.

At the bulkhead a section of the tunnel floor was removed and a water intake, fashioned from aluminium honeycomb, was inserted. At the far downstream end of the flume a weir was installed to control the water level. During operation a small steady stream of water flowed into the flume and the residue from that lost by evaporation passed over the weir to a drain.

The working section was not horizontal when operating. Suppose the plane of the tunnel is adjusted so that it is horizontal, and the flume is filled with water to a level sufficient to immerse the bottom of the tunnel to the desired operating depth. After starting the fan, the air will gradually drive the water from within the tunnel. However, water can be made to stay in the tunnel by tilting the downstream end of the tunnel slightly upwards from horizontal by means of the adjusting legs, together with an upward adjustment of the weir. Both the mean water level and pressure gradient within the working section can be held constant when the tunnel is operated in this manner. Moreover, for wind speeds ranging from 3·6 to 10 m s^{-1}, the mean water level in the working section can be controlled independently of wind speed.

Measurement of air flow

Measurements of the mean velocity profile in the air stream were made by traversing a Pitot tube with flattened tip at position A in the working section. A Preston tube,

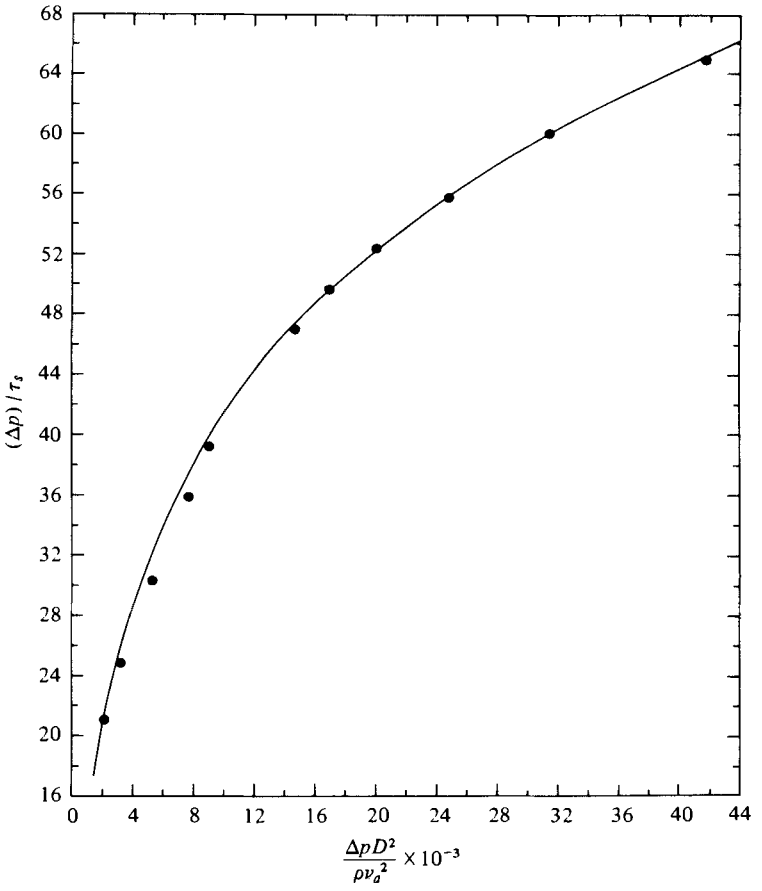

FIGURE 2. Calibration curve used for Preston tubes.

made from 0·6 mm outside diameter stainless steel tubing located at A on the upper surface of the tunnel, was used to determine the smooth wall shear stress, τ_s. The results of calibrating the tube are shown in figure 2, where $\Delta p/\tau_s$ is plotted against $\Delta p D^2/\rho \nu_a^2$, with D the outside diameter of the tube, Δp the difference between the pressure recorded by the Preston tube and the static pressure, and ν_a the kinematic viscosity of air. This presentation follows that given by Head & Ram (1971) and their tabulated values of Patel's (1965) results were used to construct the $\Delta p/\tau_s$ versus $\Delta p D^2/\rho \nu_a^2$ curve. It is evident from figure 2 that the results are in good agreement with the functional form given by Head & Ram.

Shear stress at the air–water boundary

Measurements of surface waves generated by an air flow above a film of liquid within a rectangular channel have been reported by Hanratty & Engen (1957), Lilleleht & Hanratty (1961) and Cohen & Hanratty (1968). Their method to determine the shear stress at the air–liquid boundary is based on the assumption that, for fully-developed asymmetric air flow in the channel, the positions of the plane of zero shear stress and the plane of the stationary value in the velocity profile are coincident.

However, Hanjalić & Launder (1972) measured asymmetric flows produced in a rectangular channel and observed significant separation between the plane of zero shear stress and the maximum mean velocity. Their results therefore indicate that the method used by Hanratty and co-workers is suspect.

In the working section of the wind–wave tunnel used in this study a fully-developed turbulent shear flow of air generates a stationary homogeneous wave field on water of constant mean depth. The co-ordinate system used to describe the air–water flow has its origin in the mean free water surface with x directed downstream and z directed upwards normal to x. The upper and lower boundary of the channel in contact with the air and water respectively are assumed aerodynamically smooth, the mean velocity of the air stream, u, will have an asymmetric distribution about the plane of maximum velocity.

A momentum balance of the air stream in the x direction yields the following relationships,

$$-a\,dp/dx = \tau_s, \quad -b\,dp/dx = \tau_w, \tag{3), (4}$$

where a and b are the distances from the plane of zero shear stress to the smooth wall and mean free water surface respectively, and dp/dx is the static pressure gradient. Since τ_s can be obtained from the Preston tube, and the total channel height H, mean depth of water d, and dp/dx can each be measured, then equations (3) and (4) may be used to determine τ_w.

Wave measuring system

A number of wave probes were developed during the course of the present study. These include probes to sense water depth, wave elevation and wave slope, and probes to measure two point spatial correlations. All the probes relied on sensing changes in the capacitance of enamel-coated wires caused by variation in water elevation. The capacitance changes of the probes were detected with Tektronix type 3C66 Carrier Amplifiers. The sensitivity selected for most experiments was 1·5 V mm^{-1} change in water level, but for all the wave slope measurements 3 V mm^{-1} was used. A full description of the performance of the probes is given in Lleonart (1975).

Calibration

Static calibration of the probes was performed by accurately varying their depth of immersion in still water. The influence of moisture absorbed by the enamel insulation on the wire was tested and it was shown that, if the wires were immersed in water for about four hours prior to calibration, then changes were negligible thereafter. Linearity between the output voltage and water depth was good over a range exceeding the largest wave heights encountered during the experiments.

Spindel & Schultheiss (1971) tested a capacitance-type wave measuring system, the frequency response of which they describe as flat to well over 100 Hz. In order to explore the accuracy of the probes when subject to high frequency waves they were tested as follows. A probe made from 0·05 mm outside diameter wire was attached to the underside of, and close to, the free end of a cantilever beam. The wave probe was partly immersed in a small container of water. Facing the top surface of the beam, but not touching it, was clamped the probe of a Wayne Kerr Vibration meter with its axis aligned with the vertical wire of the wave probe.

The output voltages of the wave probe and the vibration meter were filtered by a

Dytronics 723 Multi-Character Filter set up to serve as a pair of identical low pass filters. Both signals were then fed to a dual trace storage oscilloscope. The sensitivity of each channel was adjusted so that identical outputs were observed when the beam was given a static deflexion. The frequency response of the vibration meters is flat over a range exceeding that required of the wave probe. By adjusting the length of the beam the desired frequency of vibration could be obtained. An impulsive displacement of about 0·5 mm was applied to the end of the beam and the signals from the probes were simultaneously stored on the oscilloscope. It was possible to carry out tests for frequencies between 230 and 1000 Hz and it was found that the motion sensed by the wave probe agreed with that of the beam.

Probes

The mean depth of water in the working section of the wind–wave tunnel was monitored continuously at stations A and B during experimental runs. Two identical probes were mounted in the top wall of the tunnel; the sensing element used was enamel-coated copper wire with outside diameter 0·1 mm. For measuring surface elevation a similar wire of 0·05 mm outside diameter was used as a sensor. The probe was located at position A and the foot of the probe support fitted neatly into a small recess in the tunnel floor in order to eliminate flow distortion.

The probes used to measure two-point spatial correlations of surface elevation differ slightly from those described above. Because it was necessary that the probes be manoeuvrable in the working section, the wire sensor was attached to a support fashioned from a fine needle. The eye of the needle was filled with epoxy resin and a small hole drilled in it to anchor the wire. This construction allowed the needle supports to be located close to the floor of the channel while causing relatively slight distortion to the flow near the bottom.

The probe signal was fed from the amplifier to a high-pass filter of cut-off frequency 0·3 Hz. High frequency noise was removed by a low-pass filter with a cut-off frequency of 900 Hz. The resulting signal was recorded on a Electro-data Associates FM tape recorder, and its r.m.s. value read on a Bruel and Kjaer random noise voltmeter. Particular attention was necessary to shield probes from electrical interference. Measurement of noise level from the signal of a probe operating in still water revealed an r.m.s. voltage of 13 mV. Typical r.m.s. output voltages from the probe when set up to measure surface elevation in various wind-generated wave fields ranged from 0·7 to 1·5 V.

Measurement of slope

To measure the instantaneous slope of the wave surface two closely-spaced parallel wires were attached to the same probe frame. The wires were mounted vertically and in operation each sensed the water elevation. The slope was determined by feeding the output signals to an analog computer where their instantaneous difference was obtained and then multiplied by a constant representing the reciprocal of the distance between the wires. For the slope probe 0·05 mm outside diameter enamelled wire was used, and the sensitivity of the individual wires was 3 $\mathrm{V mm^{-1}}$.

Before settling on a final design for the probe, a prototype with a wire separation of 0·4 mm was constructed and studied by ciné film while operating in actual wind waves. This was done by mounting the probe in a small tank and a flow of air from a nozzle was

used to generate steep capillary waves with crests running approximately normal to the plane of the probe wires. Filming was done with a Fastax high speed ciné camera fitted with a telescopic lens and operating at 2000 frames per second. A number of sequences showing the action of the waves on the probe in silhouette were obtained. Figure 3 (plate 1) is a photograph made from a segment of the film; it illustrates the probe wires as they appear when measuring the slope of the water surface.

Examination of the film indicated that the interaction between the menisci formed on the wires was not significant. More importantly, the shape of the meniscus on each wire appeared to be reasonably similar; this was reassuring because the method of measuring the slope by sensing the difference in water elevation between each wire incurs less error when the menisci are similar. The film also showed that the water drains from the probe wires without distinguishable disturbances. The probe adopted for the experimental programme was similar to that described above except that the wire spacing was increased to 0·5 mm. Neglecting meniscus effects, the relative error in slope caused by finite spacing of the probe wires may be estimated for waves of sinusoidal form. The error is about 10 % for 2 mm-long waves and 0·5 mm wire spacing. Further details of the slope probes are given in Lleonart (1975). During experiments the slope probe was located at position A in the working section.

Spectral analysis

A fast Fourier Transform programme was used for spectral analysis of the recorded wave data. Each wave record was digitized and stored on magnetic tape; the sampling frequency used was 3000 samples per second. The records were about 3 minutes long and contained 2^{19} sample points. These were divided into 128 segments each of 2^{12} points, and final smoothed spectral estimates and effective resolution bandwidth were obtained using both segment averaging and frequency smoothing.

3. Results

Preliminary tests

Before commencing the main experimental programme, tests were made in order to verify the two-dimensional nature of the air flow in the dry channel. Velocity profiles were measured at four positions across the width of the channel in line with station A in the working section. No significant irregularities in the air flow were found. Mean velocity profiles were measured in the centre of the channel at station A; the results were well described by the logarithmic law.

The maximum value of the mean velocity, U_m, was used to describe the tunnel setting. During preliminary tests the tunnel was set to operate at 8 m s^{-1}. The waves generated exhibited the characteristic three-dimensional structure reported by Hanratty and co-workers; furthermore, they were similar qualitatively in profile to those predicted by Crapper (1957), displaying cusps at the trough and crests that were rounded.

In order to study the homogeneity of the wave field, amplitude spectra were recorded from a mean-depth probe at station A, then, without altering the operating conditions in the tunnel, recorded from the same probe at station B located 1·6 m upstream. The measured mean depth of water was 5·18 mm at both stations; this value was maintained in all later experimental runs.

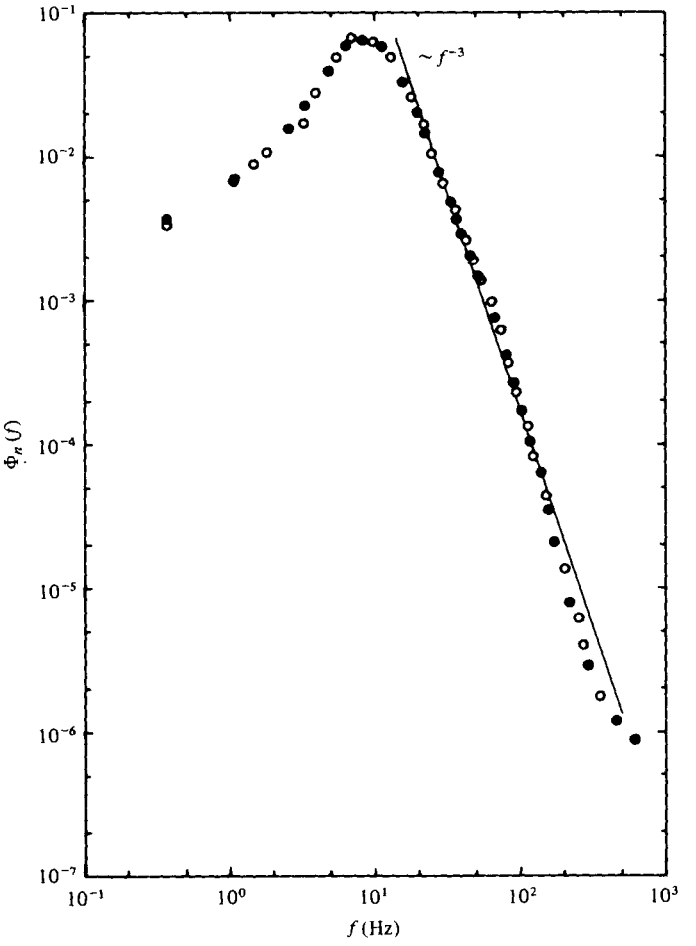

FIGURE 4. Normalized surface elevation spectra from stations A and B. ○, station A; ●, station B. $U_m = 8$ m s^{-1}.

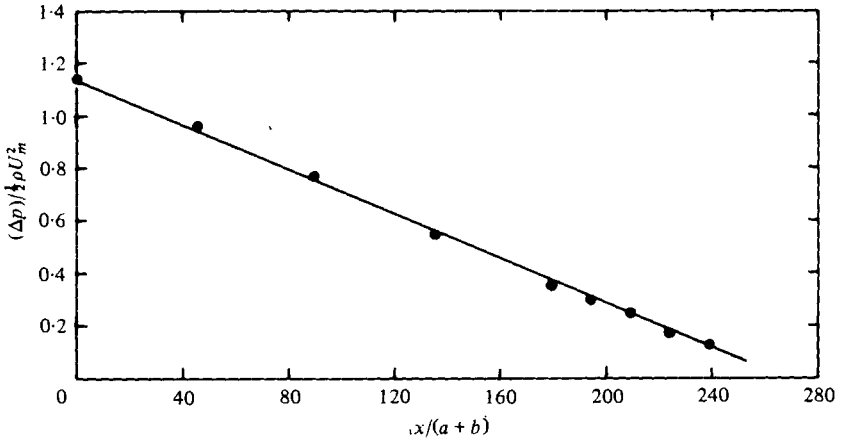

FIGURE 5. Static pressure distribution in the working section of the wind–wave tunnel. $U_m = 8$ m s^{-1}.

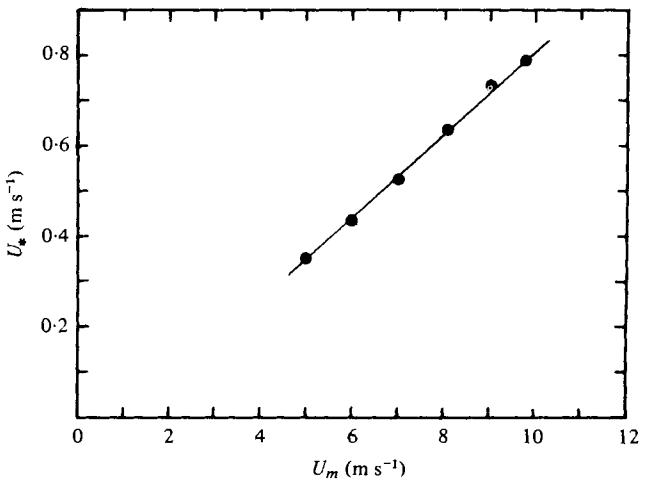

FIGURE 6. Friction velocity at the water surface as a function of wind velocity. ——, $u_* = 0{\cdot}094U_m - 0{\cdot}127$.

Identical values of r.m.s. surface elevation were observed at each station. Normalized frequency spectra, Φ_n, obtained from each station are presented for comparison in figure 4. These results indicate excellent agreement between the form of the two spectra. Clearly, the spectrum obtained from either station in the wave field cannot be distinguished according to its position. In view of these measurements it was concluded that the wave field was both stationary and homogeneous.

Since the air flow had sufficient length in which to become fully developed, it was expected that the static pressure gradient would be constant for the experimental conditions prevailing in the working section. This proved to be the case; figure 5 shows the static pressure distribution plotted as $\Delta p/\frac{1}{2}\rho U_m^2$ against $x/(a+b)$.

Friction velocity and wind speed

The friction velocity at the air–water boundary, u_*, was deduced from readings of the Preston tube and static pressure gradient along the axis of the wind–wave tunnel according to the procedure outlined above. In all, six values of u_* were obtained for the range of wind speeds 5 to 9·8 m s^{-1}. It was not possible to obtain a reliable value of u_* corresponding to 3·6 m s^{-1}. The friction velocity is well represented as a function of wind speed by a linear relation and a least squares fit yields

$$u_* = 0{\cdot}094\,U_m - 0{\cdot}127. \tag{5}$$

Figure 6 shows the experimental results.

Surface drift velocity

The surface drift velocity was estimated from the motion of floating particles released upstream. The particles used were paper disks, diameter 1 mm, the product of a paper-tape punch. These were timed over a measured distance of the working section, and the usual assumption made that they shared the true surface current. The ratio of the observed drift velocity, u_s, to the mean wind speed averaged over the whole flow, U, is shown in figure 7, plotted against a Reynolds number based on drift velocity and mean

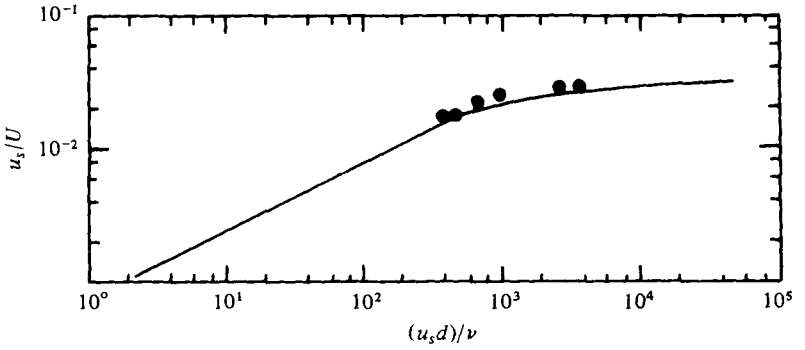

FIGURE 7. Variation of surface current with Reynolds number. ——, Keulegan (1951).

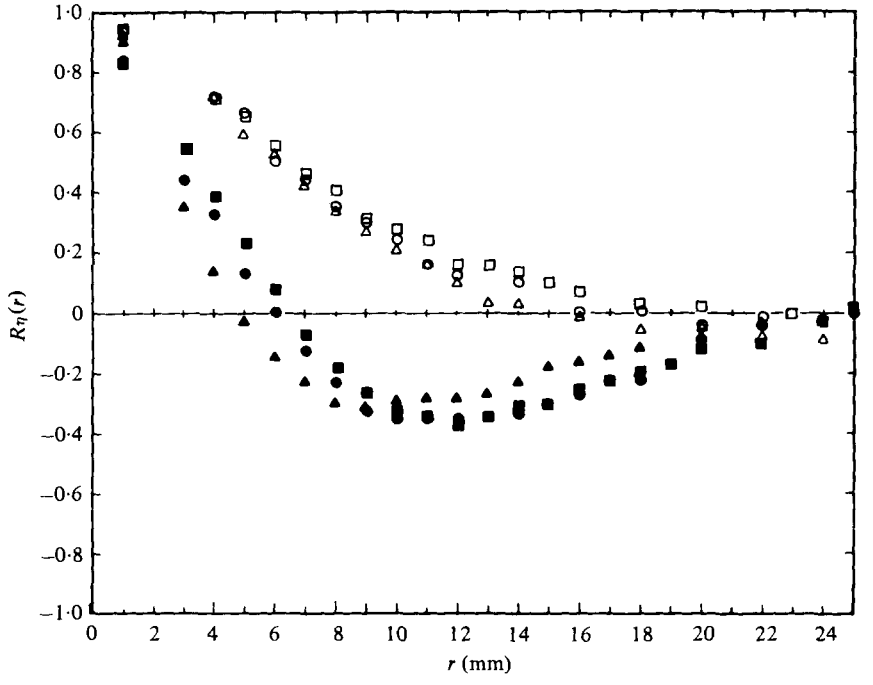

FIGURE 8. Down-wind and cross-wind spatial correlation of surface elevation. Cross-wind U_m values: □, 9 m s^{-1}; ○, 8 m s^{-1}; △, 6 m s^{-1}. Down-wind U_m values: ■, 9 m s^{-1}; ●, 8 m s^{-1}; ▲, 6 m s^{-1}.

water depth. This description has been chosen so that the results may be compared with those of Keulegan (1951); as can be seen, the agreement is satisfactory.

Correlation function of surface displacement

Measurements of the normalized spatial correlation function $R_\eta(r)$, where r is the distance separating the probes, were obtained for wind speeds of 6, 8 and 9 m s^{-1} at station A in the tunnel. The signal from each probe was passed through identical high- and low-pass filters with cut-off frequencies of 0·3 and 900 Hz respectively. The output signals were then multiplied together on an analog computer and integrated over a

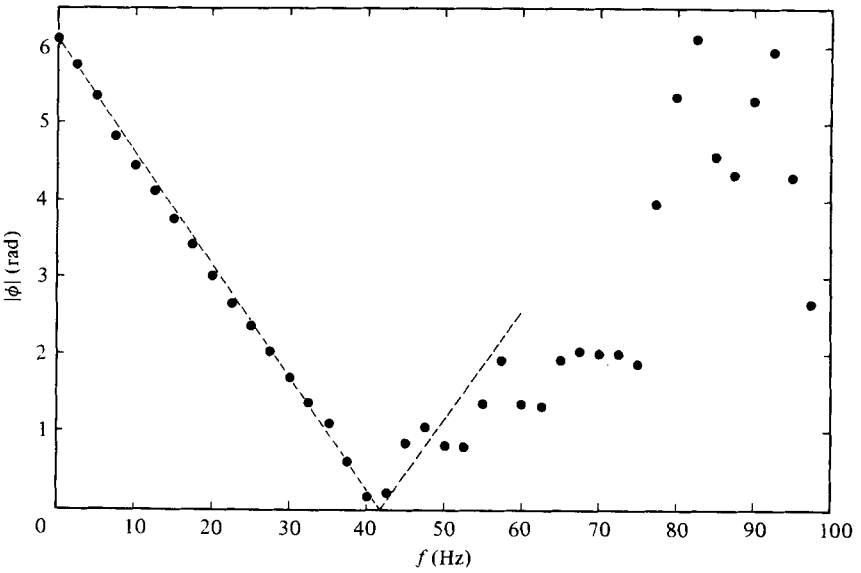

FIGURE 9. Phase component of the cross-spectral density of surface elevation as a function of frequency. U_m = 8 m s^{-1}; separation = 10 mm.

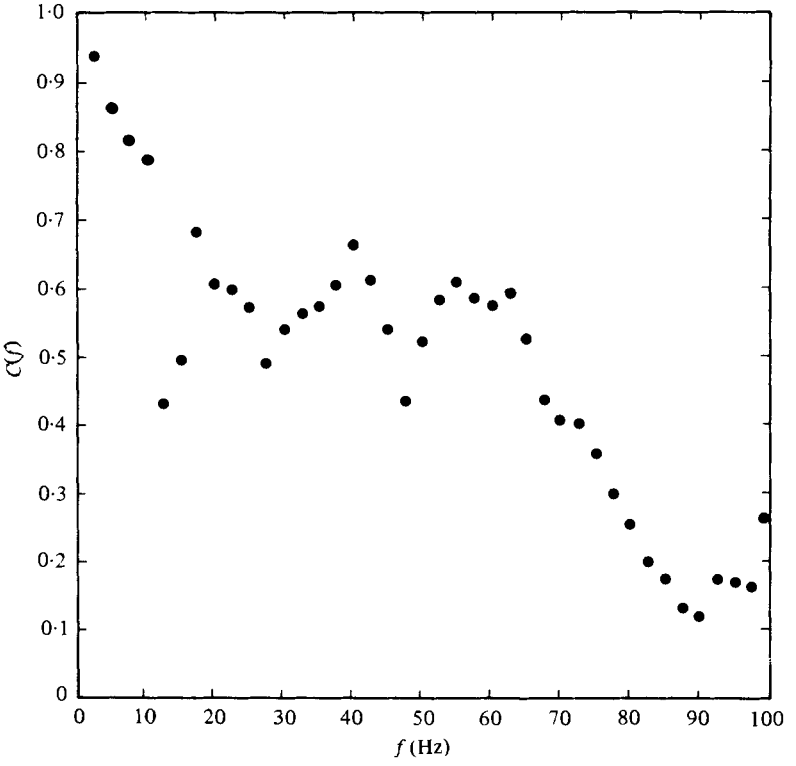

FIGURE 10. Coherence of surface elevation as a function of frequency. U_m = 8 m s^{-1}; separation 10 mm.

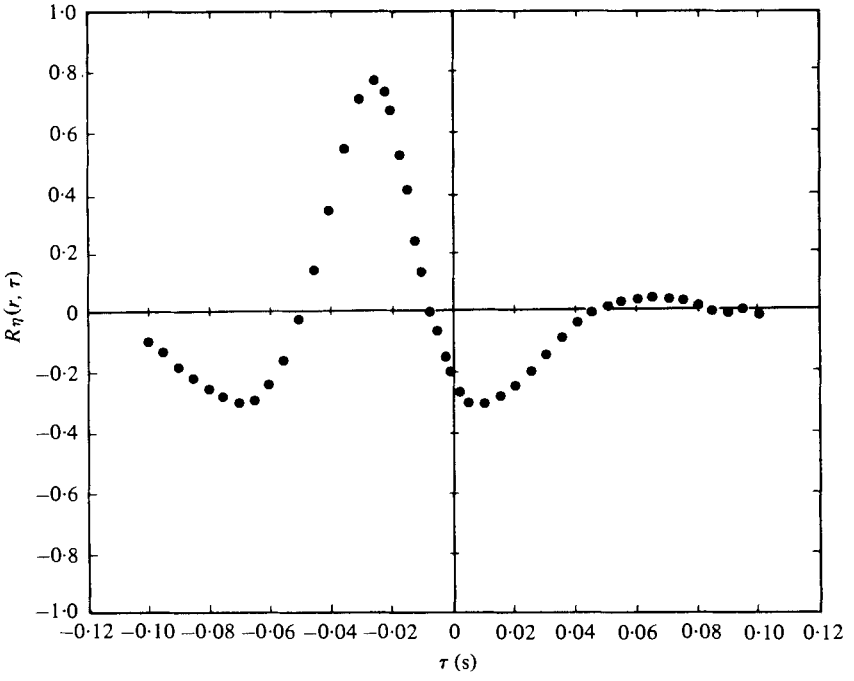

FIGURE 11. Time-delayed cross-correlation of surface elevation. $U_m = 8$ m s^{-1}; spatial separation in down-wind direction 10 mm.

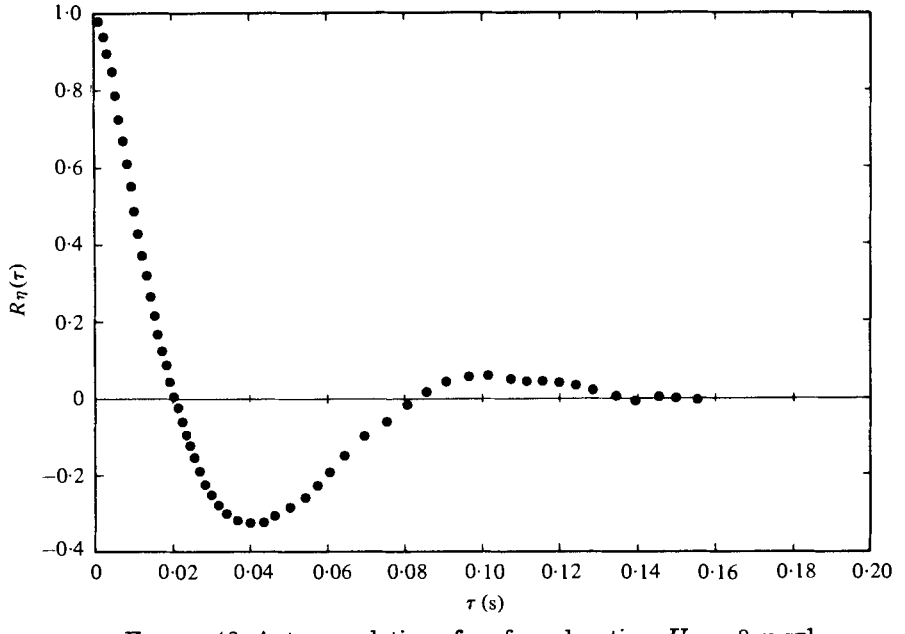

FIGURE 12. Auto-correlation of surface elevation. $U_m = 8$ m s^{-1}.

suitable time interval. The results are plotted in figure 8. In the down-wind direction, the spatial correlation exhibits quasi-periodic behaviour typical of a band-limited random process. The results for the cross-wind direction suggest no periodic behaviour.

The experimental run at 8 m s^{-1} for a down-wind separation of 10 mm was recorded and the normalized cross-correlation function, $R_\eta(r, \tau)$, where τ represents the lag in time, was computed on a PAR101 Correlator. These data were subsequently transferred to a digital computer to obtain the phase component $\phi(f)$ of the cross-spectral density between the two probes as a function of frequency, f, and additionally the coherence $C(f)$ between the probe signals. These results are shown in figures 9 and 10. The normalized cross-correlation $R_\eta(r, \tau)$ and normalized auto-correlation $R_\eta(\tau)$ are shown plotted in figures 11 and 12.

Examination of the phase–frequency graph, figure 9, shows that ϕ is linearly related to f for the frequency range $0{\cdot}3 < f < 50$ Hz. This indicates that wave dispersion is negligible and that the waves can reasonably be assumed to propagate in a frozen pattern. The variation of coherence with frequency, figure 10, indicates that waves of frequency about 10 Hz are strongly coherent. However, this function drops off rapidly with frequency and this is reflected in the phase–frequency relation which tends to a constant value of phase as the higher frequency components become uncorrelated.

For waves propagating in a frozen pattern, the auto-correlation and space-correlation coefficients should be related through the convection velocity of the pattern, U_c, by the equation

$$R_\eta(0, \tau) = R_\eta(U_c \tau, 0). \tag{6}$$

Inspection of the spatial and auto-correlations for a wind speed of 8 m s^{-1}, plotted in figures 8 and 12, shows them to be similar, and $R_\eta(r)$ and $R_\eta(\tau)$ can be brought into reasonable coincidence in this case if $U_c = 0{\cdot}30$ m s^{-1}. Another estimate may be obtained from the cross-correlation function shown in figure 11. A signal received from the first probe is received at the second probe, distance r_m downstream, at time τ_m later. The value of $R_\eta(r_m, \tau_m)$ should then be a maximum and the value of U_c is given by r_m/τ_m. Values read from figure 11 indicate that U_c is approximately $0{\cdot}37$ m s^{-1}. The agreement between these estimates of U_c is only fair and evidently a more comprehensive study of this particular aspect is needed.

An estimate of the wavelength of the dominant frequency components of the wave-field for a wind of 8 m s^{-1} may be made by studying the spatial correlation curve or, under the assumption of a frozen wave pattern, the corresponding auto-correlation curve. It turns out that this wavelength is about 2·4 cm.

Spectral measurements of the waves

Records of surface elevation and of down-wind and cross-wind wave surface slope were obtained for a range of wind speeds varying from 3·6 to 9·8 m s^{-1}. The results for the surface elevation spectrum, Φ, have been plotted against frequency in figure 13. For frequencies greater than 15 Hz there appeared to be a region of the spectrum which exhibited a dependence closely proportional to f^{-3}. However, no equilibrium range in the spectral density, in the sense that it was independent of wind speed, was evident.

The down-wind slope spectra S_{11} are plotted against frequency in figure 14. Except for the lowest wind speed, the down-wind spectra show a range of frequencies that vary as f^{-1}; this is in accord with the results of Cox (1958) and of Long & Huang

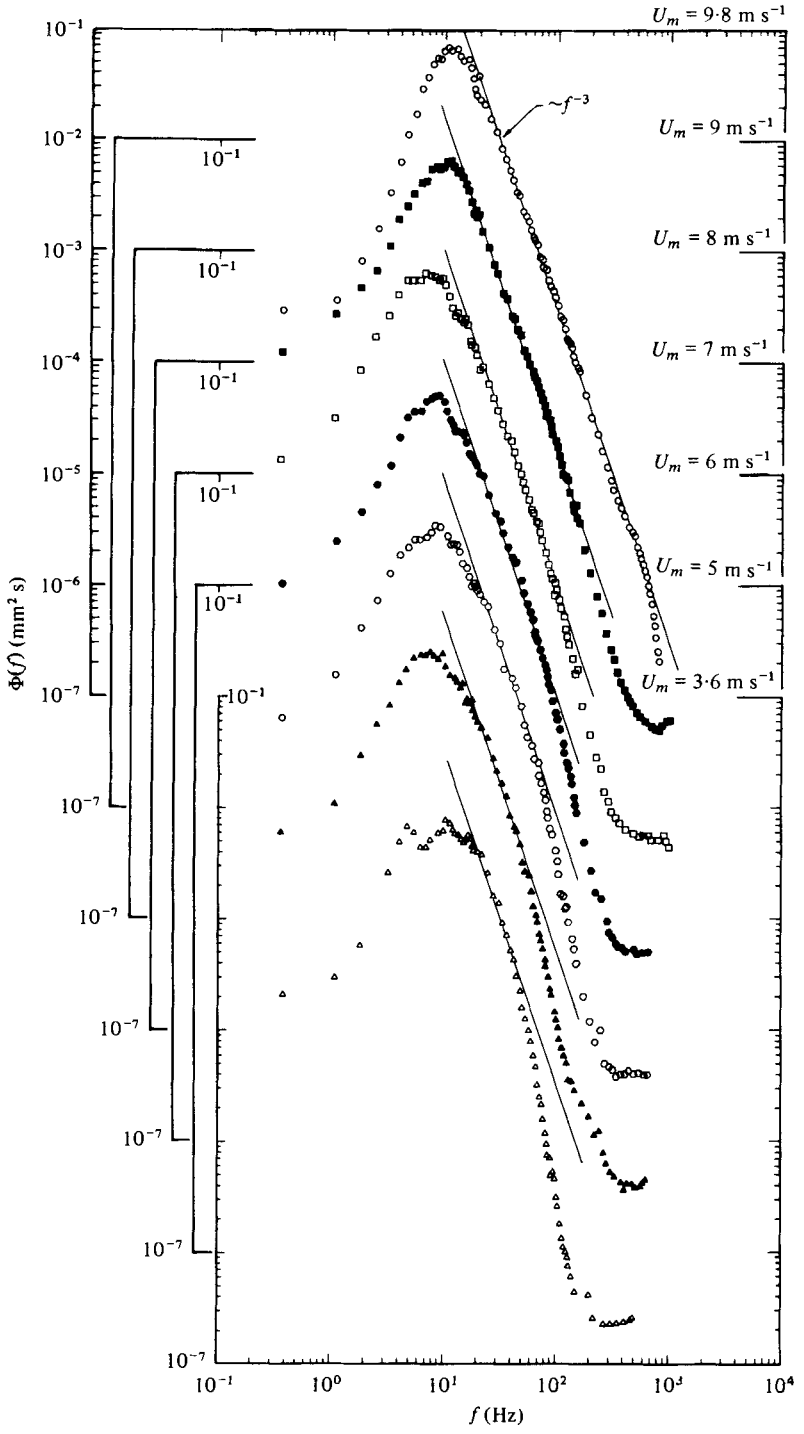

FIGURE 13. Unnormalized spectra of surface elevation. U_m values: ○, 9·8 m s^{-1}; ■, 9 m s^{-1}; □, 8 m s^{-1}; ●, 7 m s^{-1}; ○, 6 m s^{-1}; ▲, 5 m s^{-1}; △, 3·6 m s^{-1}.

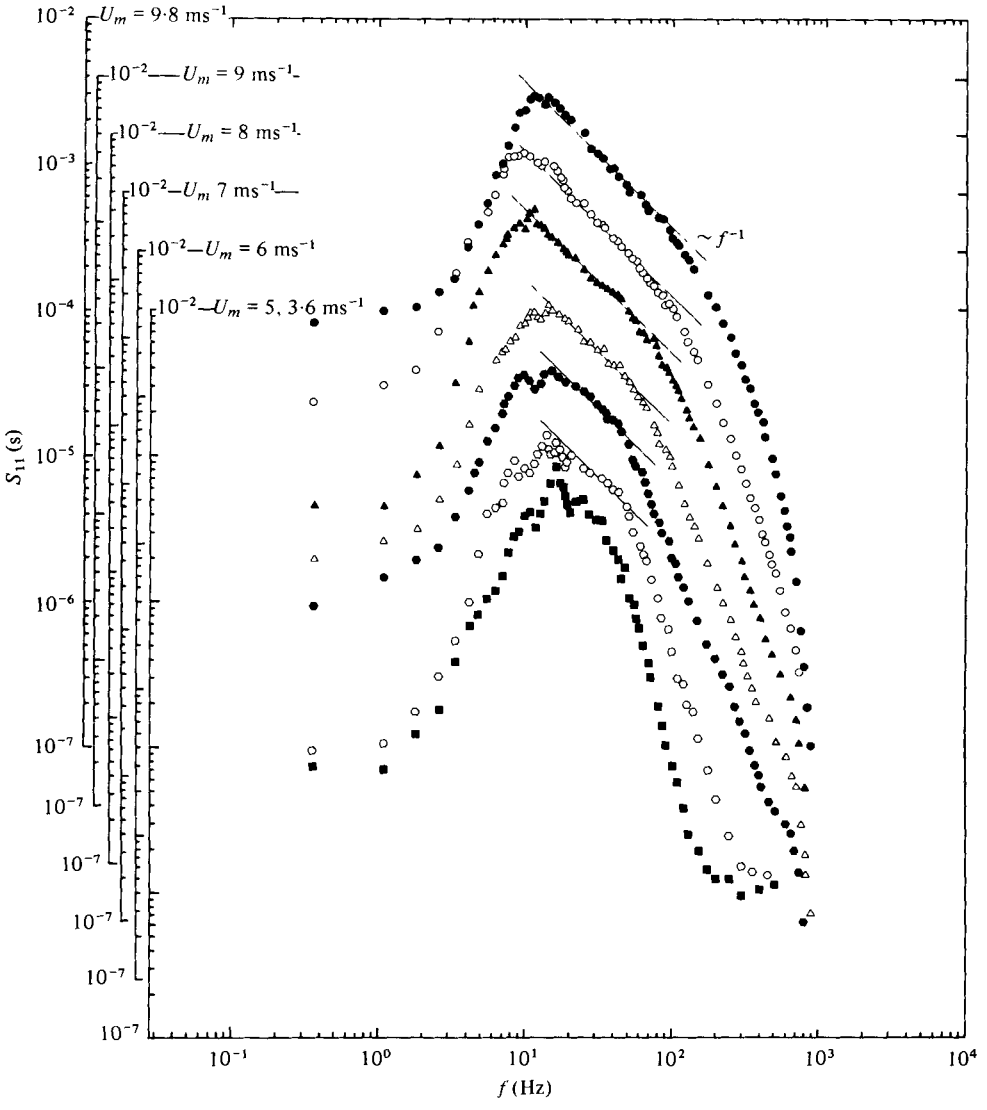

FIGURE 14. Unnormalized spectra of surface slope. U_m values: ●, 9·8 m s^{-1}: ○, 9 m s^{-1}; ▲, 8 m s^{-1}; △, 7 m s^{-1}; ⬣, 6 m s^{-1}; ⬡, 5 m s^{-1}; ■, 3·6 m s^{-1}.

(1976). As with the amplitude spectra, the spectral density of the down-wind slope also appears to show a dependence on wind speed. In figure 15 cross-wind slope spectra have been plotted in the form fS_{22} versus f. For the higher wind speeds the weighted cross-wind spectra show a small but distinct plateau, thus they are similar in form to the down-wind spectra. It is clear, however, that S_{11} and S_{22} are not independent of wind speed.

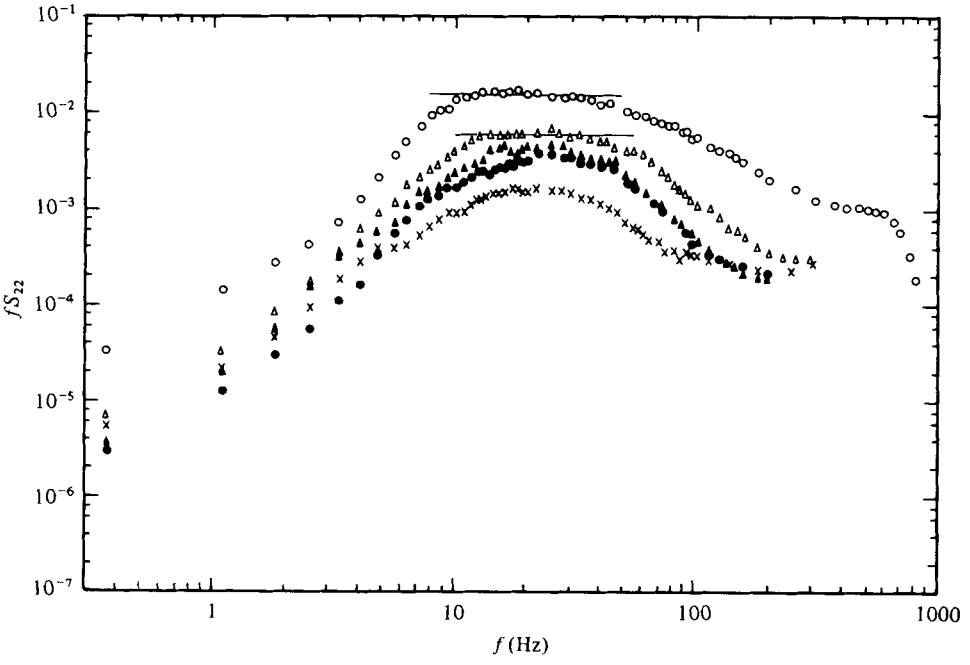

FIGURE 15. Frequency-weighted spectra of cross-wind surface slope. U_m values: ○, 9 m s^{-1}; △, 7 m s^{-1}; ▲, 6 m s^{-1}; ●, 5 m s^{-1}; ×, 3·6 m s^{-1}.

4. Capillary wave spectra

Phillips (1966) made use of an equilibrium range hypothesis to derive equations describing the spectral characteristics of wind-generated capillary waves. According to this hypothesis, the surface-elevation spectrum $\Phi(\omega)$ is determined by the angular frequency of the waves, ω and by γ, the surface tension of the fluid divided by its density. Thus, by dimensional analysis

$$\Phi(\omega) = \beta\gamma^{\frac{3}{2}}\omega^{-\frac{7}{2}}, \tag{7}$$

where β is a constant. This equation was originally attributed to Hicks (see Phillips 1966).

The data that are available neither support the frequency dependence in (7) nor verify that an equilibrium range as envisaged exists. Kondo, Fujinawa & Naito (1973) have observed ocean waves of high frequency using a capacitance wave probe. The results of their investigation suggest that a saturation limit for the capillary range of wave frequencies does not exist. A laboratory study of high frequency waves was reported by Mitsuyasu & Honda (1974). In that study, capillary wave spectra were shown to be strongly wind dependent and no evidence of an upper limit in spectral density was found.

Phillips (1958) was careful to point out that predictions concerning the shape of the capillary wave spectrum under the saturation conditions of the equilibrium range hypothesis may not be fulfilled because the influence of viscosity could be significant. In following up this suggestion, we take the view that the failure of the foregoing

equation to describe adequately an equilibrium range in the frequency spectrum is a consequence of omitting viscosity and friction velocity from the analysis.

We consider the parameters that determine the frequency spectrum of wave elevation in a wave field containing a range of frequency components $\omega_\gamma < \omega < \omega_\nu$, where ω_γ represents the frequency above which surface tension is the dominant influence on the waves, and ω_ν is the frequency beyond which the wave components are rapidly dissipated by viscosity. Both ω_γ and ω_ν are as yet undetermined, but we expect $\omega_\gamma \gtrsim (4g^3/\gamma)^{\frac{1}{4}}$. It is postulated that the rate at which these waves gain energy from the wind, q, depends on parameters which characterize the associated wind and wave fields. These parameters are u_* and γ. Since the dimensions of q are energy per unit time per unit mass $[L^2T^{-3}]$, by dimensional reasoning

$$q = Au_*^5/\gamma, \tag{8}$$

where A is a constant. We further assume that there is significant viscous dissipation of energy by the waves, and include ν; the only other parameter is ω. Thus the functional form of the spectrum is

$$\Phi(\omega) = f_1(q, \nu, \omega). \tag{9}$$

Using dimensional analysis this may be written as

$$\Phi(\omega) = D'\frac{\nu^2}{q}\left(\frac{\nu^{\frac{1}{2}}\omega}{q^{\frac{1}{2}}}\right)^n, \tag{10}$$

where D' is a constant.

It is possible to evaluate the exponent n in (10) by developing an alternative expression for $\Phi(\omega)$ in terms of the parameters u^*, ω, T and μ where T is the surface tension and μ the absolute viscosity of the water. Once more using dimensional analysis and using now mass, length and time as fundamental dimensions we obtain

$$\Phi(\omega) = D''u_*^2\,\omega^{-3}(u^*\mu/T)^m = D''u_*^2\,\omega^{-3}(u^*\nu/\gamma)^m. \tag{11}$$

Combining (10) and (11) gives $n = -3$ and $m = \frac{1}{2}$; therefore rewriting (10) or (11) in terms of frequency $f\,(= 2\pi/\omega)$ yields

$$\Phi(f) = Du_*^2\left(\frac{u_*\,\nu}{\gamma}\right)^{\frac{1}{2}} f^{-3}, \tag{12}$$

where D is a constant.

An equilibrium range in the spectrum of wave surface slope was also proposed by Phillips (1966). For capillary waves the saturated frequency spectrum, S_{ij}, was thought to depend only on ω and γ: thus by dimensional analysis

$$S_{ij}(\omega) = C_{ij}\omega^{-1}, \tag{13}$$

where C_{ij} are constant with i and j equal to 1 or 2 according to whether the slope component is in the down-wind or cross-wind direction.

Laboratory measurements of capillary wave surface slope were made by Cox (1958) using an optical-refraction technique. The results obtained indicated an approximate ω^{-1} region within each spectrum; however, it is doubtful whether the spectra are independent of wind speed. More recently, Long & Huang (1976) used a laser to make wave surface slope measurements in the capillary–gravity range. Their results show S_{ij} depending on ω^{-1} in the capillary range of the spectrum; although they found the

shape of the spectrum similar for each wind speed, its magnitude showed some variation. It appears therefore that (13) does not completely describe an equilibrium range in the capillary wave slope spectrum.

An expression describing the form of the down-wind wave slope spectrum within the frequency range $\omega_\gamma < \omega < \omega_\nu$ may be found by making use of equation (12). Denoting the displacements from the mean free surface by η, we define the following auto-correlation functions of the waves at one fixed point as a function of time t:

surface elevation

$$B_\eta(\tau) = B_\eta(0,\tau) = \overline{\eta(x,t) \times \eta(x,t+\tau)}; \tag{14}$$

slope of the wave surface

$$B_{\eta'}(\tau) = B_{\eta'}(0,\tau) = \overline{\frac{\partial \eta}{\partial x}(x,t) \times \frac{\partial \eta}{\partial x}(x,t+\tau)}; \tag{15}$$

and vertical velocity of the surface

$$B_{\dot{\eta}}(\tau) = B_{\dot{\eta}}(0,\tau) = \overline{\frac{\partial \eta}{\partial t}(x,t) \times \frac{\partial \eta}{\partial t}(x,t+\tau)}. \tag{16}$$

The results of our cross-correlation experiment suggest that the range of waves we are concerned with are non-dispersive and, to a good approximation, frequency may be related to wavenumber by the expression

$$\omega = kU_c. \tag{17}$$

We may therefore write the instantaneous vertical velocity of the wave surface at a fixed point as

$$\partial \eta / \partial t = -U_c \, \partial \eta / \partial x, \tag{18}$$

thus the relation between (15) and (16) is

$$B_{\dot{\eta}}(\tau) = U_c^2 B_{\eta'}. \tag{19}$$

B_η and $B_{\eta'}$ can be expressed in terms of their respective spectra:

$$B_\eta = \frac{1}{2\pi} \int_{-\infty}^{\infty} \Phi(\omega) \, e^{i\omega\tau} d\omega; \tag{20}$$

$$B_{\eta'} = \frac{1}{2\pi} \int_{-\infty}^{\infty} S_{11}(\omega) \, e^{i\omega\tau} \, d\omega. \tag{21}$$

Using the well-known identity

$$B_{\dot{\eta}} = -\frac{d^2}{d\tau^2} [B_\eta(\tau)], \tag{22}$$

in conjunction with the above equations it follows that

$$S_{11}(\omega) = (\omega / U_c)^2 \, \Phi(\omega). \tag{23}$$

If the wave disturbed surface behaves essentially as an aerodynamically rough surface, the mean rate of working, W, of the wind stress on a column of water of unit area is given approximately by

$$W \sim \tau_w u_*. \tag{24}$$

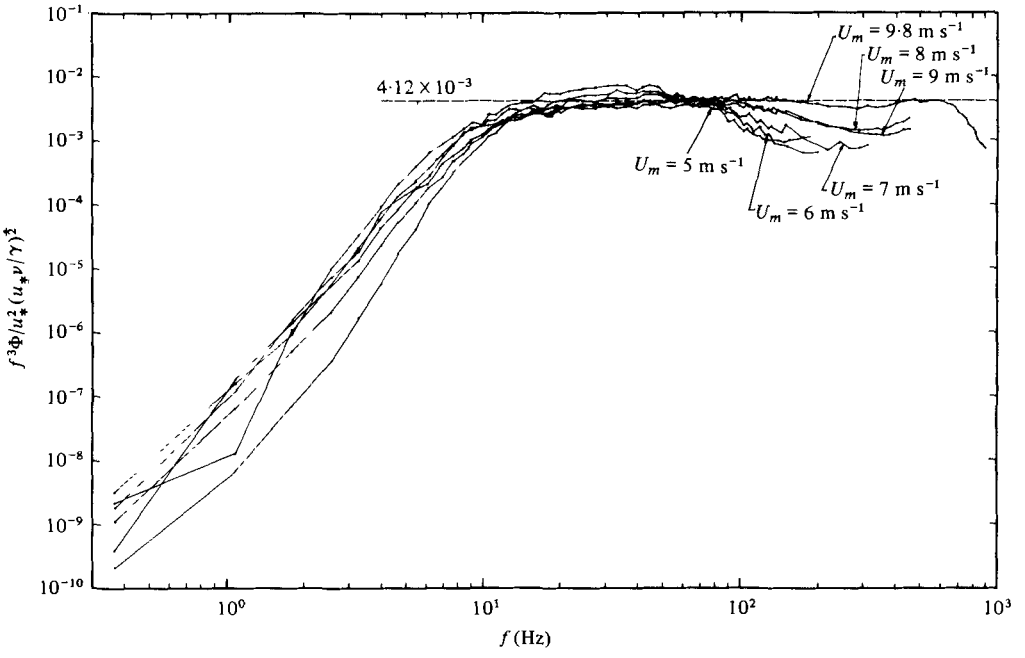

FIGURE 16. Normalized spectra of surface elevation.

Stewart & Grant (1962) have argued that an estimate of the rate of energy input to waves can be found by taking the product of the rate of momentum input to the waves and some mean wave phase speed. By adopting this concept in the form

$$W \sim \tau_w U_c, \tag{25}$$

equations (24) and (25) lead us to expect that u_* is approximately proportional to U_c. Melville (1977) presents alternative arguments that support the proposition that $u_* \approx U_c$. With the aid of this estimate for U_c, equation (23) assumes the form

$$S_{11}(f) = C_{11}(u_*\nu/\gamma)^{\frac{1}{2}} f^{-1} \tag{26}$$

where C_{11} is a constant.

5. Discussion

As proposed above, an equilibrium range in the capillary wave spectrum which accounts for wind speed may exist. The data were processed to test equation (12) and the results are plotted as $f^3\Phi/u_*^2(u_*\nu/\gamma)^{\frac{1}{2}}$ versus f in figure 16. The spectrum corresponding to the lowest wind speed was not included because of doubt regarding the reality of the f^{-3} region and uncertainty in the value of u_*. The range of the spectrum which is proportional to f^{-3} extends from about 15 to 200 Hz for U_m = 9·8 m s^{-1}. For the spectra obtained at other wind speeds the lower frequency limit is also close to 15 Hz; the upper frequency limit is, however, clearly wind-speed dependent and for the range of wind speed studied it appears to vary from about 80 to 200 Hz. All the spectra show a decrease in spectral density with frequency which is greater than f^{-3} for the frequencies beyond the upper limit of the f^{-3} region. The spectral density of this region

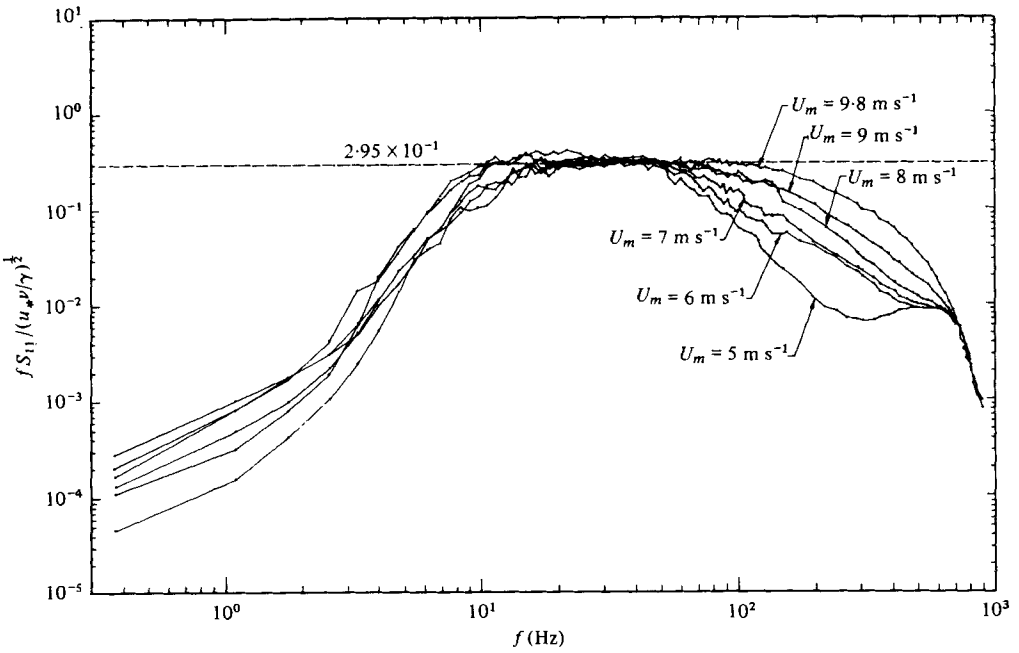

FIGURE 17. Normalized spectra of down-wind surface slope.

beyond the equilibrium range presumably diminishes more rapidly with frequency because the wave components affected by viscosity cannot be sustained by the wind.

The surface slope observations were re-plotted to check whether equation (26) would represent the data. These results are shown in figure 17, plotted in the form

$$fS_{11}/(u_* \nu/\gamma)^{\frac{1}{2}} \quad \text{versus} \quad f.$$

It can be seen that equation (26) provides a good description of a region of the down-wind slope spectra. Therefore, the experimental observations lend weight to the proposal that an equilibrium range as previously described actually exists. The weighted spectra show several features previously noted by Cox. The width of the plateau evident in the spectra increases with wind speed. For the highest wind speeds the extent of the plateau ranges from approximately 15 to 90 Hz. In the present study, the spectral density does not show the peak at lower frequencies found in the measurements of Cox and of Long & Huang. This may be because the wind–wave tunnel tends to suppress the growth of the longer gravity waves. Beyond the f^{-1} region the spectral density falls off rapidly. No attempt was made to combine the parameters u_*, γ and ν with S_{22}.

The value of the constant D in (12) was computed by considering spectral values judged to be within an f^{-3} region. For the surface elevation spectra, 214 values were used. The mean and standard deviation of D were found to be $4{\cdot}12 \times 10^{-3}$ and $8{\cdot}7 \times 10^{-4}$ respectively: the standard error of the mean is therefore $\pm 5{\cdot}9 \times 10^{-5}$. The constant C_{11} in (26) was similarly determined from 207 spectral values falling within the f^{-1} region and the mean and standard deviation were $2{\cdot}95 \times 10^{-1}$ and $4{\cdot}1 \times 10^{-2}$ respectively; the standard error of the mean is $\pm 2{\cdot}8 \times 10^{-3}$.

Reliable experimental data on high frequency wave spectra are very limited and

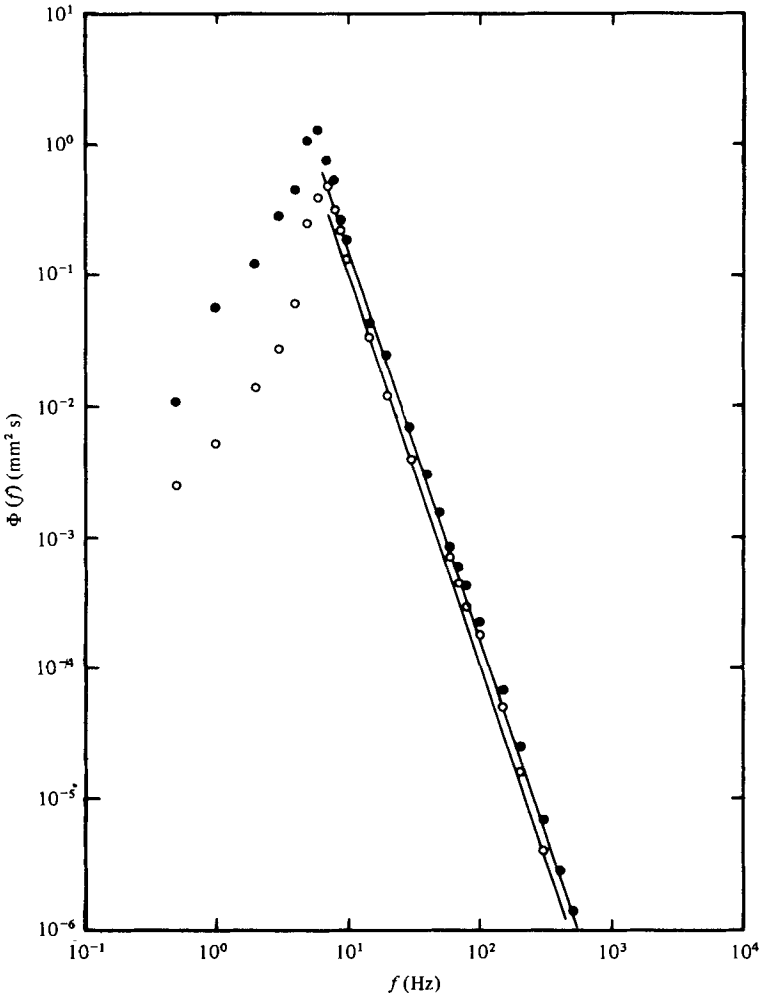

FIGURE 18. Surface elevation spectra of Mahomet (1973) compared with equation (12). Fetch = 70 cm. ●, $u_* = 0{\cdot}585$ m s^{-1}; ○, $u_* = 0{\cdot}490$ m s^{-1}. The lines represent equation (12).

few fruitful comparisons with other studies are possible. Mahomet (1973), working in our laboratory, investigated the frequency dependence of capillary wave surface elevation spectra with the same wave probes as used in this study. His measurements were made at short fetches in deep water (60 cm) by modifying the existing wind–wave tunnel. The amplitude spectra reported by him all contained a region in which Φ was proportional to f^{-3}, except for the lowest wind speed case. Mahomet also measured the friction velocity in his study, so that a useful comparison with his spectra was possible. Data taken from the graphs he presented were plotted in accordance with equation (12). Figure 18 shows the results and it appears that there is good agreement with the present results.

Another experimental study, by Mitsuyasu & Honda (1974), concerns the high frequency spectrum of wind waves in the laboratory. The authors thoroughly tested their wave recording system and the measurements were carried out under carefully

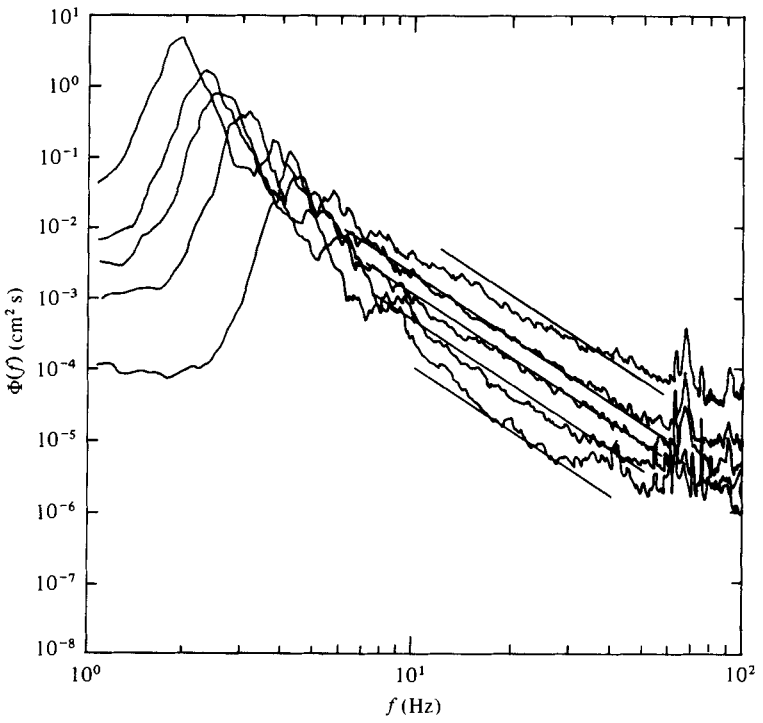

FIGURE 19. Surface elevation spectra of Mitsuyasu & Honda (1974) compared with equation (12). Fetch = 825 cm, wind speeds = 5, 7·5, 10, 12·5 and 15 m s^{-1}.

controlled conditions. Values of u_* were obtained from wind profile measurements. Figure 11 of their paper is reproduced in figure 19. With the exception of the spectrum corresponding to the highest wind speed (15 m s^{-1}) which, as the authors pointed out, was influenced by spray, it can be seen that for frequencies greater than about 15 Hz there exists a region of the surface elevation spectra which is in modest agreement with the f^{-3} law. The solid lines drawn in figure 19 represent equation (12). There is very fair agreement with the present results. The mean value of the friction velocity $\overline{u}_*$, which was deduced from measured values of the local friction velocity at stations within a fetch, were used in (12). These values were given in table 1 of Mitsuyasu & Honda's paper and were found to correlate the data better than when u_* was used. While u_* may characterize the local interaction between the air flow and the wave field, the spectrum itself is influenced by the total upstream wind field. Therefore, it seems reasonable to use $\overline{u}_*$ when the spectrum is developing with fetch as was the case in the experiments referred to above.

On the basis of the measurements by Mahomet and by Mitsuyasu & Honda it also appears, as was suggested earlier, that the limited water depth used in our experiments does not markedly influence the spectral values for the range of frequencies described by (12).

Chang (1968) measured wind wave spectra in the laboratory and presented two amplitude spectra which in the capillary range of frequencies he found varied as f^{-3}. Chang did not measure u_* in his experiments but determined it from an empirical formula given by Hidy & Plate (1966). When compared with equation (12) Chang's

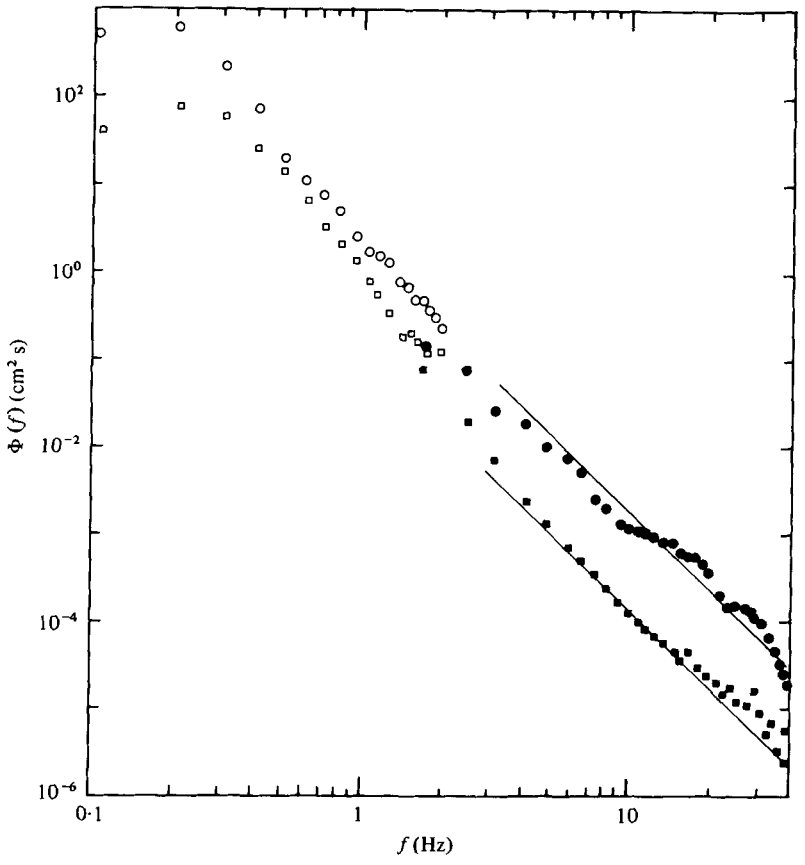

FIGURE 20. Surface elevation spectra of Kondo *et al.* (1973) compared with equation (12). ○, ●, Kondo's run 37; □, ■, run 74.

spectra show a significant discrepancy. The wind–wave tunnels used by Chang and by Mitsuyasu & Honda are similar in both cross-section and fetch dimensions. It is, however, puzzling to compare the spectra obtained from each tunnel on the basis of the given friction velocities. Chang's 'case 1' spectrum, which corresponds to $u_* = 0{\cdot}395$ m s^{-1}, falls somewhat below the spectral density of Mitsuyasu & Honda's lowest wind speed spectrum which corresponds to $u_* = 0{\cdot}259$ m s^{-1} or $\bar{u}_* = 0{\cdot}212$ m s^{-1}. A similar discrepancy appears to exist for Chang's 'case 2' spectrum.

In another laboratory study of high frequency waves generated by air flow above a thin liquid film, Lilleleht & Hanratty (1961) measured wave spectra using a light absorption technique. Their dimensional analysis neglects surface tension and viscosity in favour of gravity, but includes friction velocity. This is surely incorrect, since surface tension should be more significant than gravity for the small wavelengths reported in their experiments. The data were plotted by them in the form $\Phi g^3/u_*^5$ versus fu_*/g. The f^{-5} law, favoured as representing the high frequency region of the spectra, was later reported by Cohen (1964) to be atypical. No comparisons have been attempted with the spectra of either Lilleleht & Hanratty (1961) or Cohen (1964) since there appears to be considerable variation in the form of the individual spectra.

A study of high frequency waves in the ocean was reported by Kondo *et al.* (1973). They found that there was a significant dependence of Φ on wind speed for the capillary wave region of the spectrum. Figure 3 of Kondo's paper is shown here as figure 20, and a line representing equation (12) has been added to the high frequency region of the spectra. The values of u_* used in (12) were obtained from the wind stress correlation graph given by Wu (1960). When compared with the data, (12) provides rather marginal agreement. However, the observations were made in waves which were sometimes breaking so spray and air entrainment could have influenced the spectral form.

Besides the observations of Cox (1958) and of Long & Huang (1976) we know of no other spectral measurements of capillary-wave surface slope. Since Cox has not given values of u_* corresponding to the wind speeds used in his experiments useful comparisons with his work are not possible in terms of equation (26). Nevertheless, we have compared the present data qualitatively with that of Cox, and that of Long & Huang, and found reasonable agreement regarding the general form of fS_{11} within the capillary wave range of the spectrum. Long & Huang's spectral values are a good deal higher than the others in the plateau region of fS_{11} and seem questionable to us since the integrated values of S_{11} appear to be greater than the mean square slope values shown in figure 9 of their paper.

In our observations the lower frequency limit for which equations (12) and (26) appear to apply is about 15 Hz. The range of frequencies over which these equations extend is limited by the wind-dependent viscous cut-off frequency, f_ν. At the same wind speed the values of f_ν as read from the surface elevation and slope spectra are different. For example, from the surface-elevation spectrum at $U_m = 9{\cdot}8$ m s^{-1}, f_ν is approximately 200 Hz; but at the same wind speed the down-wind slope spectrum indicates that f_ν is about 90 Hz. It seems plausible that f_ν describes the same frequency limit for both Φ and S_{11}. We believe that the discrepancy is due to the inability to obtain accurate measurements with the surface slope probe at small wavelengths.

6. Conclusion

The results of this study suggest that, for the high frequency components of capillary waves, the spectra of surface elevation and slope are functions of wind speed. They do not, therefore, support the idea that the spectrum represents an equilibrium between the local energy flux from the wind to the waves and the dissipation of energy due to surface tension forces. By including friction velocity and viscosity, however, the experimental results obtained here and by some others are found to be represented by spectra of the form $Du_*^2(u_*\nu/\gamma)^{\frac{1}{2}}f^{-3}$ for surface elevation and $C_{11}(u_*\nu/\gamma)^{\frac{1}{2}}f^{-1}$ for surface slope for $15 < f < f_\nu$ Hz. The numerical values of D and C_{11} are estimated to be $4{\cdot}12 \times 10^{-3}$ and $0{\cdot}295$ respectively.

REFERENCES

CHANG, P. 1968 Laboratory measurements of air flow over wind waves following the moving water surface. *Colorado State Univ. Tech. Rep.* CER68-69 PcC18.

COHEN, L. S. 1964 Interaction between turbulent air and a flowing liquid film. Ph.D. thesis in Chem. Engng, Urbana, University of Illinois.

COHEN, L. S. & HANRATTY, T. J. 1968 Effect of waves at a gas–liquid interface on a turbulent air flow. *J. Fluid Mech.* **31**, 467–479.

COX, C. S. 1958 Measurements of slopes of high-frequency wind waves. *J. Mar. Res.* **16**, 199–225.

CRAPPER, G. D. 1957 An exact solution for progressive capillary waves of arbitrary amplitude. *J. Fluid Mech.* **2**, 532–540.

HANJALIĆ, K. & LAUNDER, B. E. 1972 Fully developed asymmetric flow in a plane channel. *J. Fluid Mech.* **51**, 301–335.

HANRATTY, T. J. & ENGEN, J. M. 1957 Interaction between a turbulent air stream and a moving water surface. *A.I.Ch.E. J.* **3**, 299–304.

HEAD, M. R. & RAM, V. V. 1971 Simplified presentation of Preston tube calibration. *Aeronaut. Q.* **22**, 295–303.

HIDY, G. M. & PLATE, E. J. 1966 Wind action on water standing in a laboratory channel. *J. Fluid Mech.* **26**, 651–687.

KEULEGAN, G. H. 1951 Wind tides in small closed channels. *J. Res. Nat. Bur. Stand.* **46**, 358–381.

KONDO, J., FUJINAWA, Y. & NAITO, G. 1973 High frequency components of ocean waves and their relation to the aerodynamic roughness. *J. Phys. Oceanogr.* **3**, 197–202.

LILLELEHT, L. U. & HANRATTY, T. J. 1961 Measurement of interfacial structure for co-current air–water flow. *J. Fluid Mech.* **11**, 65–81.

LLEONART, G. T. 1975 A laboratory study of wind-generated capillary waves. Ph.D. thesis, Monash University.

LONG, S. R. & HUANG, N. E. 1976 On the variation and growth of wave-slope spectra in the capillary-gravity range with increasing wind. *J. Fluid Mech.* **77**, 209–228.

MAHOMET, N. 1973 A laboratory study of wind-induced capillary–gravity waves. Dept. Mech. Engng 4th Yr. Project, Monash University.

MELVILLE, W. K. 1977 Wind stress and roughness length over breaking waves. *J. Phys. Oceanogr.* **7**, 702–710.

MITSUYASU, H. & HONDA, T. 1974 The high frequency spectrum of wind generated waves. *J. Oceanogr. Soc. Japan* **30**, 185–198.

PATEL, V. C. 1965 Calibration of the Preston tube and its limitations on its use in pressure gradients. *J. Fluid Mech.* **23**, 185–208.

PHILLIPS, O. M. 1958 Comments on paper by Dr. Cox. *J. Mar. Res.* **16**, 226–230.

PHILLIPS, O. M. 1966 *The Dynamics of the Upper Ocean.* Cambridge University Press.

SPINDEL, R. C. & SCHULTHEISS, P. M. 1971 Two-dimensional probability structure of wind-driven waves. *J. acous. Soc. Am.* **52**, 1065–1068.

STEWART, R. W. & GRANT, H. L. 1962 Determination of the rate of dissipation of turbulent energy near the sea surface in the presence of waves. *J. Geophys. Res.* **67**, 3177–3180.

WU, J. 1969 Wind stress and surface roughness at air–sea interface. *J. Geophys. Res.* **74**, 444–455.

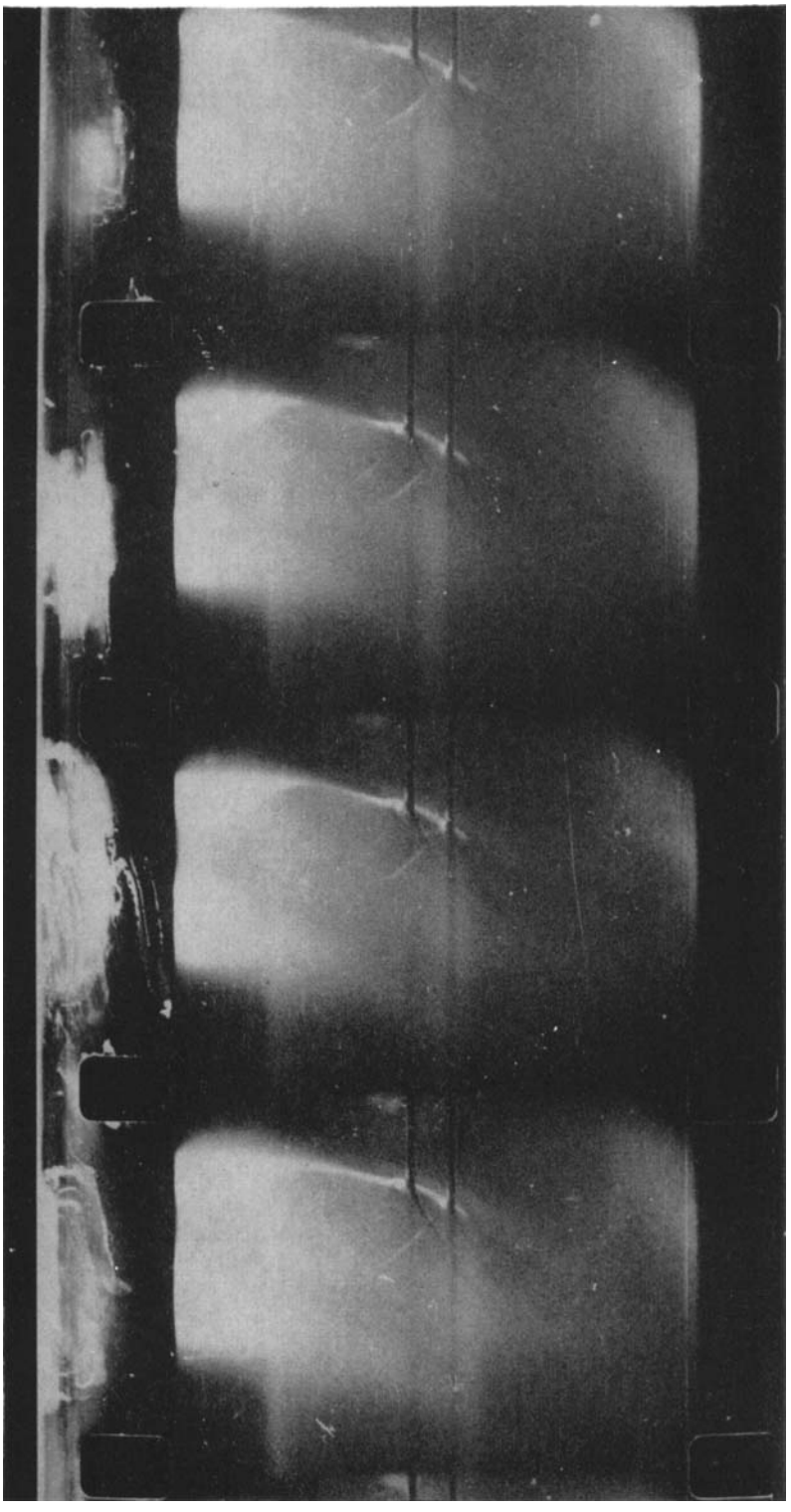

FIGURE 3. Meniscus around the wires of a surface slope probe whilst operating in a wind-generated capillary wave field. Wire diameter 0·05 mm, wire separation 0·4 mm, camera speed 2000 f.p.s.

LLEONART AND BLACKMAN (*Facing p.* 480)